Drug Design, Development and Therapy

Dovepress
open access to scientific and medical research

Open Access Full Text Article

ORIGINAL RESEARCH

Integrating Network Pharmacology and Experimental Validation to Explore the Pharmacological Mechanism of Astragaloside IV in Treating Bleomycin-Induced Pulmonary Fibrosis

Su Yuan[1,2], Biao Zuo[2,3], Si-Cong Zhou[1,2], Meng Wang[2,3], Kai-Yue Tan[2,3], Zhi-Wei Chen[2,3], Wen-Fu Cao[1–3]

[1]Department of Combination of Chinese and Western Medicine, the First Affiliated Hospital of Chongqing Medical University, Chongqing, People's Republic of China; [2]Chongqing Key Laboratory of Traditional Chinese Medicine for Prevention and Cure of Metabolic Diseases, Chongqing, People's Republic of China; [3]College of Traditional Chinese Medicine, Chongqing Medical University, Chongqing, People's Republic of China

Correspondence: Wen-Fu Cao, The First Affiliated Hospital of Chongqing Medical University, No. 1, Youyi Road, Yuanjiagang, Yuzhong District, Chongqing, 400016, People's Republic of China, Email caowenfu20220401@163.com

Purpose: Our study aims to reveal the pharmacological mechanism of Astragaloside IV in the treatment of pulmonary fibrosis(PF) through network pharmacology and experimental validation.

Methods: We first determined the in vivo anti-pulmonary fibrosis effect of Astragaloside IV by HE, MASSON staining, and lung coefficients, then used network pharmacology to predict the signaling pathways and molecularly docked key pathway proteins, and finally validated the results by in vivo and in vitro experiments.

Results: In in vivo experiments, we found that Astragaloside IV improved body weight ($P < 0.05$), increased lung coefficients ($P < 0.05$), and reduced lung inflammation and collagen deposition in mice with pulmonary fibrosis. The network pharmacology results showed that Astragaloside IV had 104 cross-targets with idiopathic pulmonary fibrosis, and the results of KEGG enrichment analysis indicated that cellular senescence could be an important pathway for Astragaloside IV in the treatment of pulmonary fibrosis. Astragaloside IV also bound well to senescence-associated proteins, according to molecular docking results. The results of both in vivo and in vitro experiments showed that Astragaloside IV significantly inhibited senescence protein markers such as P53, P21, and P16 and delayed cellular senescence ($P < 0.05$). In in vivo experiments, we also found that Astragaloside IV reduced the production of SASPs ($P < 0.05$), and in in vitro experiments, Astragaloside IV also reduced the production of ROS. In addition, by detecting epithelial-mesenchymal transition (EMT)-related marker protein expression, we also found that Astragaloside IV significantly inhibited the development of EMT in both in vivo and in vitro experiments ($P < 0.05$).

Conclusion: Our research found that Astragaloside IV could alleviate bleomycin-induced PF by preventing cellular senescence and EMT.

Keywords: astragaloside IV, pulmonary fibrosis, network pharmacology, cellular senescence, epithelial-mesenchymal transition

Introduction

Idiopathic pulmonary fibrosis (IPF) affects the lung parenchyma and is characterized by a decline in lung functions, abnormal deposition of extracellular matrix, and interstitial fibrosis that worsens with time.[1,2] The incidence of PF has been rising year after year in recent years;[3] however, IPF's onset and progression have complex mechanisms that are still unknown.[4–6] In addition to the recognized risk factors for IPF, such as smoke, environmental elements, comorbidities, and viral infections, various other processes are associated with the disease. Aging, epithelial-mesenchymal transition (EMT), endothelial-mesenchymal transfer, and epithelial cell migration are important factors in IPF-related tissue remodeling.[7] Pulmonary fibrosis (PF) is difficult to diagnose and incurable in the early stages and the prognosis is poor, with a 5-year survival <30% and an average survival time following diagnosis of 2–3 years.[8,9] Moreover, the incidence of PF is gradually increasing worldwide.[10] Nevertheless, there is a lack of effective drug therapy for IPF.

Received: 30 January 2023
Accepted: 14 April 2023
Published: 27 April 2023

Therefore, we need to urgently explore the exact molecular mechanisms of IPF progression for developing new therapeutic approaches.

Astragaloside-IV (AS-IV) is a cycloartane triterpenoid and a key active compound of *Astragalus*. It exerts numerous medicinal uses, such as anti-inflammatory, antifibrotic, antiasthmatic, antidiabetic, and immunoregulatory through various signaling channels.[11] Current research and clinical experience indicate that AS-IV has a wide range of potential applications in several diseases. For instance, it slows the advancement of renal fibrosis by inhibiting the TGF-β/Smad signaling pathway.[12] In addition, AS-IV significantly delays the progression of liver fibrosis through the PAR2 signaling pathway.[13] Moreover, it prevents cardiac fibrosis by modulating TRPM7 channels.[14] Nonetheless, the mechanism by which AS-IV impacts PF is not well established.

Network pharmacology is a developing field of research that combines bioinformatics and pharmacological methods to analyze the relationship between drugs and diseases.[15] Recently, it is primarily used to analyze the possible mechanisms of action of pharmaceuticals, which is a crucial and useful tool for pharmacological research.[16] Therefore, in this study, we combined network pharmacology with molecular docking and molecular dynamics simulations to reveal the potential targets of AS-IV on pulmonary fibrosis, and furthermore, we used in vivo and in vitro experiments to validate the relevant pharmacological mechanisms.

Materials and Methods

Drugs and Reagents

AS-IV (purity ≥98.0%) was purchased from Nanjing Dilger Medical Technology (Nanjing, China). Bleomycin was procured from Hisun Pfizer pharmaceutical company (Hangzhou, China). Prednisone acetate (Pn) was purchased from China Central Pharmaceutical Co (Xiangyang, China). TGF-β1 (ab50036), anti-α-SMA (ab124964), anti-GAPDH (ab181602), anti-TGF-β1 (ab215715), anti-Vimentin (ab92547), anti-p21 (ab109199), and anti-p16 (ab51243) were obtained from Abcam (Waltham, MA, USA). Collagen I (E8I9Z) was obtained from Cell Signaling Technology (Danvers, MA, USA). E-Cadherin (20874-1-AP) and p53 (10442-1-AP) were purchased from Proteintech (Wuhan, China). Hydroxyproline Assay Kit (HYP) was obtained from Nanjing Jiancheng Bio-Engineering Institute (Nanjing, China). Carboxymethylcellulose (CMC) solution was purchased from Leagene Biotechnology (Beijing, China). TGF-β1 ELISA kit was purchased from MULTI SCIENCES (Hangzhou, China) and the IL-6 ELISA kit was purchased from Thermo Fisher Scientific (Grand Island, NY, USA). Senescence β-Galactosidase Staining kit, Cell Counting Kit-8 (CCK-8), and ROS kit were obtained from Beyotime (Shanghai, China).

Animal Model and Treatment

We purchased 6–8-week-old male C57BL/6J mice from the Experimental Animal Center of Chongqing Medical University and kept them in a pathogen-free environment at Chongqing Medical University's animal laboratory. Food and water were freely accessible, and 12-hour light/dark cycles were maintained throughout the experiment. We established a mouse lung fibrosis model, through a tracheotomy injection of bleomycin at a dose of 5 mg/kg. Then, the mice were randomly divided into five groups: control group (Con), bleomycin group (BLM), 50 mg/kg AS-IV group (ASL), 100 mg/kg AS-IV group (ASH), and 5mg/kg positive drug group (Pn) with five mice in each group (n = 5). In terms of modeling, bleomycin was injected tracheally into all groups except the Con, which received saline. AS-IV was dissolved in 0.5% CMC sodium solution and equal amounts of CMC solution were administered to the Con and BLM groups for 28 days. The ASL and ASH groups were administered the corresponding doses of AS-IV continuously for 28 days. The Pn group was administered the corresponding dose of prednisone continuously for 28 days.

All experiments strictly followed the ethical standards (ethics committee numbers: 2022-K258). All protocols were approved by the Ethics Committee of The First Affiliated Hospital of Chongqing Medical University (Chongqing, China).

Network Pharmacology

Target Prediction of AS-IV and Collection of PF-Related Genes

The chemical structural formula of AS-IV was obtained from the ChemSpider database[17] and its potential targets were obtained from the Pharmmapper database (http://www.lilab-ecust.cn/pharmmapper/) with a maximum generated conformation of 300 and "Norm Fit" ≥0.5 was selected as a predicted target for AS-IV.[18] The PF-related genes were searched from the GeneCards (http://www.genecards.org) database[19] using the keyword "idiopathic pulmonary fibrosis." The intersection of the pharmaceutical and disease targets identified the intersecting (common) genes.

Protein–Protein Interaction Network and Core Subnetwork

We established a PPI network of the common AS-IV and PF targets with the help of the STRING database (https://cn.string-db.org/).[20] After setting the parameters to medium confidence = 0.4, the PPI network was put into Cytoscape (version 3.9.1). Next, we used a Cytoscape plugin CytoHubba to analyze the PPI network and filtered the top 10 genes using the "DMNC" ranking method and constructed sub-networks.[21]

KEGG Pathway and GO Enrichment Analyses

We used the Metascape database (www.metascape.org/) for GO and KEGG enrichment analyses of the common AS-IV and PF-related genes.[22] Further, we determined the enriched KEGG pathways of the top 10 genes using KEGG database (http://www.kegg.jp/), and the KEGG pathway maps of hub genes were derived by sorting them according to the number of related genes in the pathway.

Molecular Docking

According to KEGG analysis results, cellular senescence marker proteins p53 and p21 were selected for molecular docking with AS-IV using the CB-Dock2 tool.[23]

Molecular Dynamics Simulations

Molecular dynamics (MD) simulations were performed by GROMACS 2020.3 software. More than 1.0 nm separates the protein's atoms from the simulation box. Water molecules of density 1 fill the box and water molecules are replaced with Cl- and Na+ ions to maintain the system electrically neutral. The energy minimization operation was performed according to the steepest descent method. The NVT combination was simulated for the first-stage equilibrium at 300 K for 100 ps, and the NPT combination was simulated for the second-stage equilibrium at 1 bar and 100 ps. MD simulations were run at constant temperature and pressure (300K,101.325kPa) for 50ns.

BALF Collection in Mice

BALF was collected using previously mentioned methods.[24] The right lungs of mice were lavaged thrice with 500 μL of pre-cooled PBS, with a fluid recovery of about 80% at all times. The alveolar lavage fluid was centrifuged at 800 rpm for 5 minutes, and the supernatant was then extracted and frozen at −80°C.

Histological Analysis and Immunohistochemistry (IHC)

The lung tissues were soaked in 4% paraformaldehyde for 48 h, dehydrated in graded alcohol, embedded in paraffin, and finally cut into 5 μm thick sections. Then, the sections were stained with hematoxylin-eosin (H&E) and Masson's trichrome stain to observe lung tissue inflammation and fibrosis under a microscope (BX53, Olympus Corporation, Japan).

After endogenous peroxidase was removed from paraffin-embedded lung sections using 3% H_2O_2, the tissues were heated for antigen retrieval using citrate buffer. Subsequently, the sections were then treated to primary antibodies overnight at 4°C, followed by an hour at normal temperature in the presence of secondary antibodies. Positive staining was shown with the DAB reagent and tissues were observed under a microscope (BX53, Olympus Corporation, Japan).

Hydroxyproline (HYP) Assay

The HYP content in lung tissues is a quantitative indicator of fibrosis and was measured following reagent instructions. Briefly, a mixture of 30 mg of the tissue sample and 1 mL of the hydrolytic enzyme was heated at 60°C for 20 minutes, then 10 minutes centrifugation at 3500 rpm/min. After collecting the supernatant, its absorbance was measured at 550 nm.

Elisa

The IL-6 and TGF-β1 levels in alveolar lavage fluid and TGF-β1 levels in mouse serum were measured by the double antibody sandwich method.

Cell Culture

We purchased A549 cells from the Shanghai Cell Bank, Chinese Academy of Sciences (Shanghai, China). The cells were cultured in DMEM medium (Gibco, USA) supplemented with 10% fetal bovine serum (BI, USA) and 1x penicillin-streptomycin solution (Solarbio) at 37°C with a humid 5% CO_2 atmosphere.

Cell Viability

A549 cells (5 x 10^3 cells/well) were cultured in 96-well plates, treated with different concentrations of AS-IV for 72h, respectively; then, CCK-8 solution (10ul/well) was added and incubated for 90 min at 4°C, followed by measuring the absorbance at 450nm with a microplate reader (Biotek, USA). Cells in the experimental groups had their viability normalized to that of the cells in the control group.

Senescence-Associated β-Galactosidase (SA- β-Gal) Staining

The cells were placed in fixation solution then left at normal temperature for 15 minutes, aspirated, and then washed thrice with PBS for 3 minutes each. Then, the cells were placed in pre-formulated staining working solution at 37°C overnight. These cells were photographed through a microscope the next day.

Western Blot Analysis

We extracted total protein from lung tissues or cells using RIPA lysis buffer. The proteins were separated on 12.5% SDS-PAGE gels, followed by transfer to methanol-activated PVDF membranes (Merck Microporous, Germany) and blocked with 5% skim milk for 60 minutes. The membranes were next treated with primary antibodies for an overnight incubation at 4°C, then three TBST washes, each for 10 minutes, and incubated with the corresponding secondary antibody for 60 minutes at normal temperature. ECL (Biosharp, China) was used to visualize the blots and ImageJ 6.0 was used to evaluate the band intensity.

Detection of ROS

Treated A549 cells (5 x 10^3 cells/well) were seeded in 96-well black plates and incubated at 37°C for 72 hours. Then measured ROS levels in cells with 2,7-Dichlorofluorescin diacetate (DCFH-DA) assay. A fluorescent microscope (BX53, Olympus Corporation, Japan) was used to observe each well after DCFH-DA was added at a concentration of 10 μM and kept for 30 minutes at 37°C.

Statistical Analysis

Prism 8.0 (GraphPad Software, USA) was used for graphing and statistical analysis. Mean standard error was the only way to express all raw data. One-way ANOVA and post-hoc Tukey multiple comparison tests were used to test the Statistical significance in different samples. $P < 0.05$ was set as statistically significant.

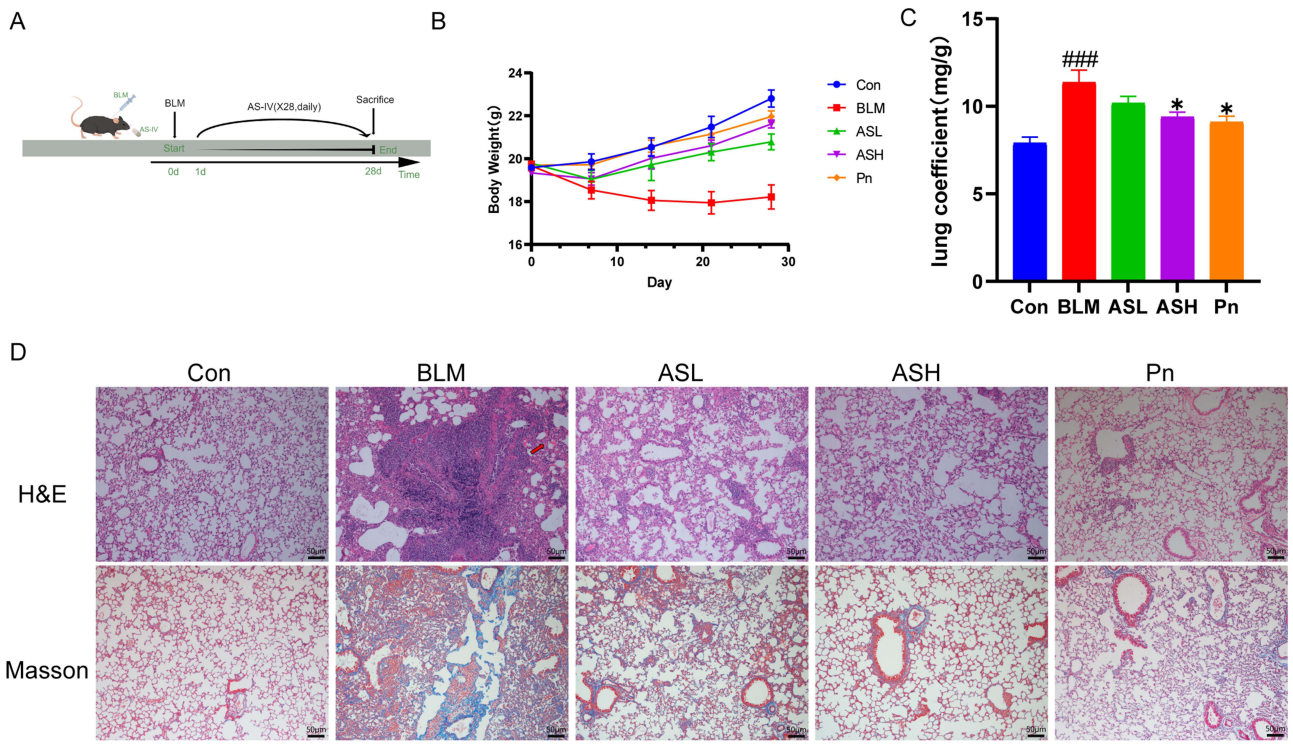

Figure 1 AS-IV ameliorates pulmonary fibrosis in mice. (**A**) Flow chart of mouse pulmonary fibrosis model. (**B**) Mouse weight chart, n = 5 for each group. (**C**) Lung coefficients of mice. (**D**) H&E and Masson staining revealed alveolar septum thickening, alveolar structural disruption, massive inflammatory cell infiltration in the alveolar lumen, and interstitium with massive collagen fiber deposition in the BLM group, which were improved by AS-IV and Pn treatment. Red arrows point to areas of alveolar septal thickening, destruction of alveolar structures, and marked inflammatory cell infiltration in the alveolar cavity and interstitium. Scale bar:50um. Results are shown as mean ± SEM (n≥3). ### $P < 0.001$, versus Con group; * $P < 0.05$, versus BLM group.

Results

AS-IV Attenuates Bleomycin-Induced PF in Mice

We used a mouse model of bleomycin-induced PF to study the antifibrotic effects of AS-IV in vivo (Figure 1A). Body weight tracking revealed that the bleomycin-induced mice lost weight quickly during the 28-day bleomycin PF trial. Meanwhile, the ASH group started to reverse this weight loss after one week and achieved roughly the same result as the Pn group (Figure 1B). The lung coefficients were notably higher in the BLM group than in the Con group. Strikingly, the ASH and Pn groups showed significantly reduced lung coefficients ($P < 0.05$) (Figure 1C). Histological analysis showed no apparent pathological changes in the lung structures of the Con and ASH groups. Instead, in the BLM group, HE staining exhibited morphological alterations in the lung tissue, including alveolar septum thickening, breakdown of alveolar structure, and significant inflammatory cell infiltration in the alveolar cavity and interstitial lungs. Additionally, Masson staining revealed that collagen sedimentation was significantly high in the lung tissues of the BLM group. According to the findings of pathological sections, ASH group considerably decreased collagen deposition, septal thickness, and inflammatory cell infiltration. The BLM group considerably exacerbated fibrosis and inflammation, while the ASH and Pn groups protected the lung microstructure (Figure 1D).

AS-IV Reduces Collagen Deposition in the Interstitial Lung of Fibrotic Mice

Collagen sedimentation is a remarkable characteristic of PF. The IHC staining of lung sections revealed that the BLM group had high collagen deposition, whereas the ASH and Pn groups had low collagen deposition (Figure 2A). Moreover, the BLM group showed a significant increase in HYP production, while the ASH group significantly inhibited HYP production at day 28 ($P < 0.05$) (Figure 2B). This suggests that AS-IV may prevent bleomycin-induced PF by decreasing collagen production. The extracellular matrix is primarily produced by myofibroblasts that secrete high amounts of collagen. We observed that mice in the ASH group had considerably low collagen 1 and α-SMA expression levels in their

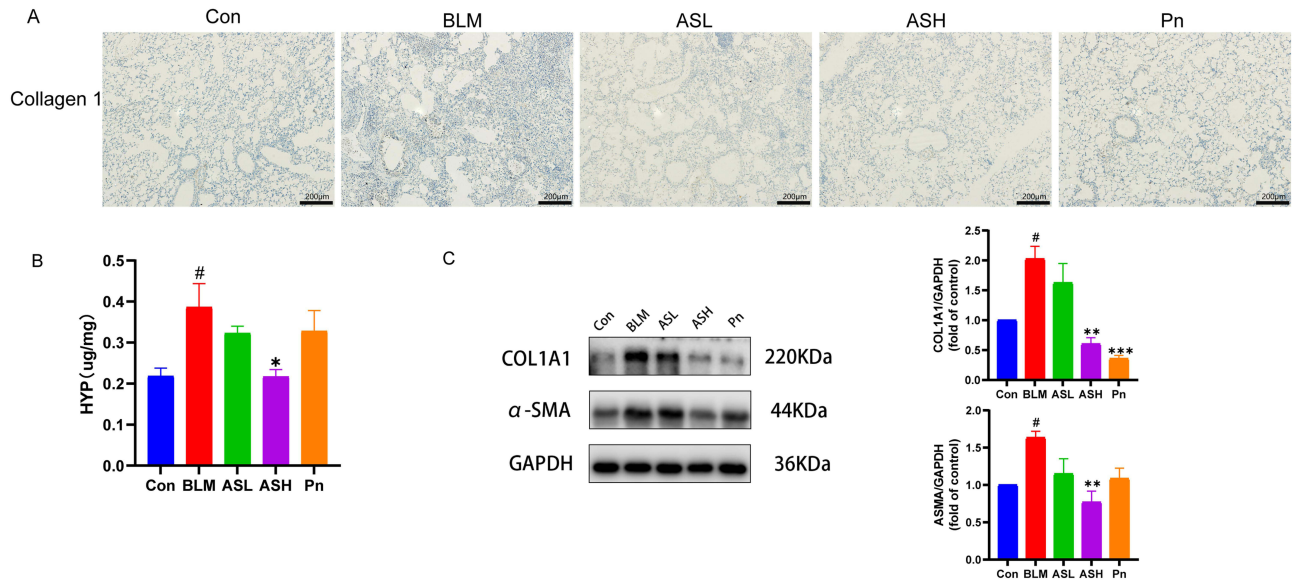

Figure 2 AS-IV reduces collagen deposition in the interstitial lung of fibrotic mice. (**A**) Immunohistochemical staining for collagen I deposition in the BLM group, which was significantly improved in the ASH and Pn groups. Scale bar:200um. (**B**) HYP levels of each group. (**C**) Western blot of collagen I(COL1A1) and α-SMA in lung tissues of fibrotic mice. Data are shown as mean ± SEM (n≥3). # P < 0.05, vs Con group; * P < 0.05, ** P < 0.01, *** P < 0.001, vs BLM group.

lung tissues (P < 0.01). This indicates that the ASH treatment may prevent fibroblasts from transdifferentiating into myofibroblasts and hence prevent collagen deposition (P < 0.01) (Figure 2C). Altogether, these results show that AS-IV mitigates the development of bleomycin-induced PF by decreasing collagen deposition.

Network Pharmacology Analysis

Drug-Disease Common Target Protein Collection

The structure of AS-IV is shown in Figure 3A. In all, 145 potential AS-IV targets and 3600 non-repetitive disease targets were identified. Finally, after intersection analysis, we obtained 104 potential AS-IV targets treating PF (Figure 3B). Constructing a PPI network graph to view relevant core targets (Figure 3C). We further used cytohubba to find the top 10 key proteins, from 1 to 10, in the order of CCNA2, HSPA8, CDK2, AURKA, CDK6, ANXA5, PARP1, CSK, MDM2, and ITK (Figure 3D).

Pathway Enrichment Analysis

GO enrichment analysis consists of three categories: biological process (BP), cellular component (CC), and molecular function (MF). We observed that the common AS-IV and PF-related genes were enriched in 20 MP, 20 BP, and 16 CC. The BP terms included protein phosphorylation, cellular response to lipids, and response to hypoxia (Figure 4A). We selected the top 20 signaling pathways associated with PF, including cellular senescence, PPAR signaling pathway, and VEGF signaling pathway (Figure 4B). Further, we noticed that the top 10 targets from Cytohubba were primarily enriched in cellular senescence pathways, it is also directly related to the cellular senescence marker proteins P53, P21, P16, and the initiation of P53, P21, P16 directly inhibits the related targets and promotes cellular senescence (Figure 4C).

Molecular Docking and Molecular Dynamics Simulation

Based on KEGG pathway enrichment results, we chose this pathway for molecular docking validation. We found that AS-IV binds to p21 and p53 with an energy of −9.8 kJ/mol and −7.8 kJ/mol, respectively. These findings showed that AS-IV has good binding affinities with both p53 and p21 (Figure 5A). We performed molecular dynamics simulations on the molecular docking results, and as shown in the Figure 5B, root-mean-square deviation(RMSD) values fluctuate less after 20 ns and the protein binds tightly to the ligand. Thus, based on pathway enrichment, molecular docking, and validation of molecular dynamics simulations, the cellular senescence pathway was chosen as a key node for the ensuing investigation.

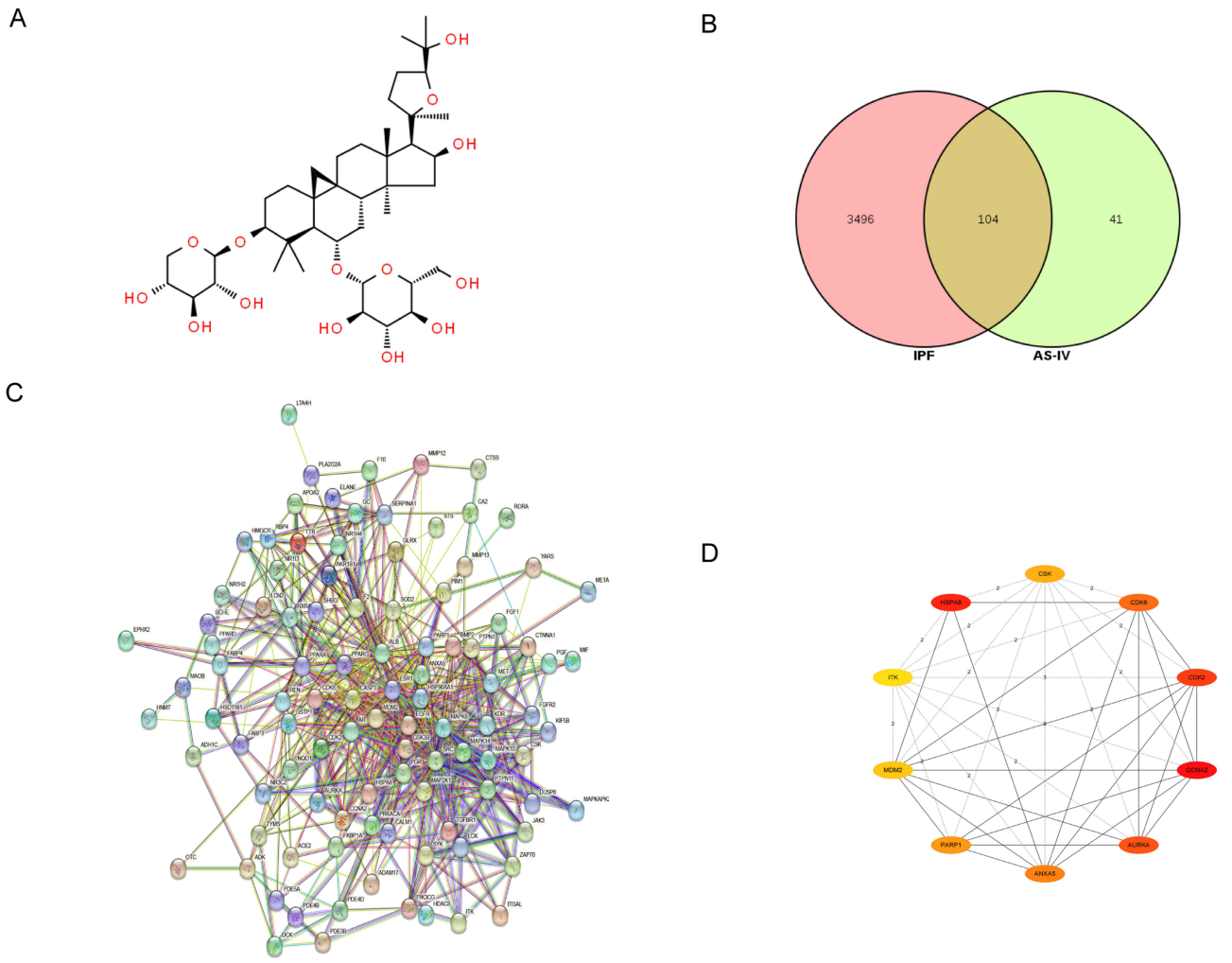

Figure 3 Network pharmacology. (**A**) Molecular structure of AS-IV. (**B**) Map of the common AS-IV and IPF targets. (**C**) PPI network of the common targets of drugs and diseases. (**D**) The top 10 targets that CytoHubba has screened.

AS-IV Attenuates Bleomycin-Induced Senescence and Inflammatory Response in Alveolar Epithelial Cells

Bleomycin effectively induces alveolar epithelial cell senescence.[25] Since p53, p21, and p16 proteins are cellular senescence markers, we tested their expression levels using Western blot. We observed that, compared with the BLM group, p53, p21, and p16 were dramatically suppressed in the ASH group ($P < 0.001$, $P < 0.01$, $P < 0.05$) (Figure 6A). Moreover, IHC staining revealed that p21 and p16 were highly expressed in the lung tissues of BLM mice, while AS-IV treatment lowered their expressions (Figure 6B).

Senescent cells secrete biologically active substances known as SASPs, which accelerates aging and has an impact on neighboring cells. Therefore, we explored the impact of AS-IV on SASPs generation using ELISA, and these cytokines are also considered to be part of inflammatory response. We observed that compared with the Con group, IL-6 and TGF-β1 levels in alveolar lavage fluid were massively high in the BLM group, whereas considerably low in the ASH group ($P < 0.01$, $P < 0.05$) (Figure 6C). In addition, the AS-IV treatment group had dramatically decreased TGF-β1 in serum compared with the BLM group, thus reducing the inflammatory response in the lungs and inhibiting PF development ($P < 0.05$) (Figure 6D). Collectively, these results reveal that AS-IV inhibits senescence and inflammation in alveolar epithelial cells in vivo.

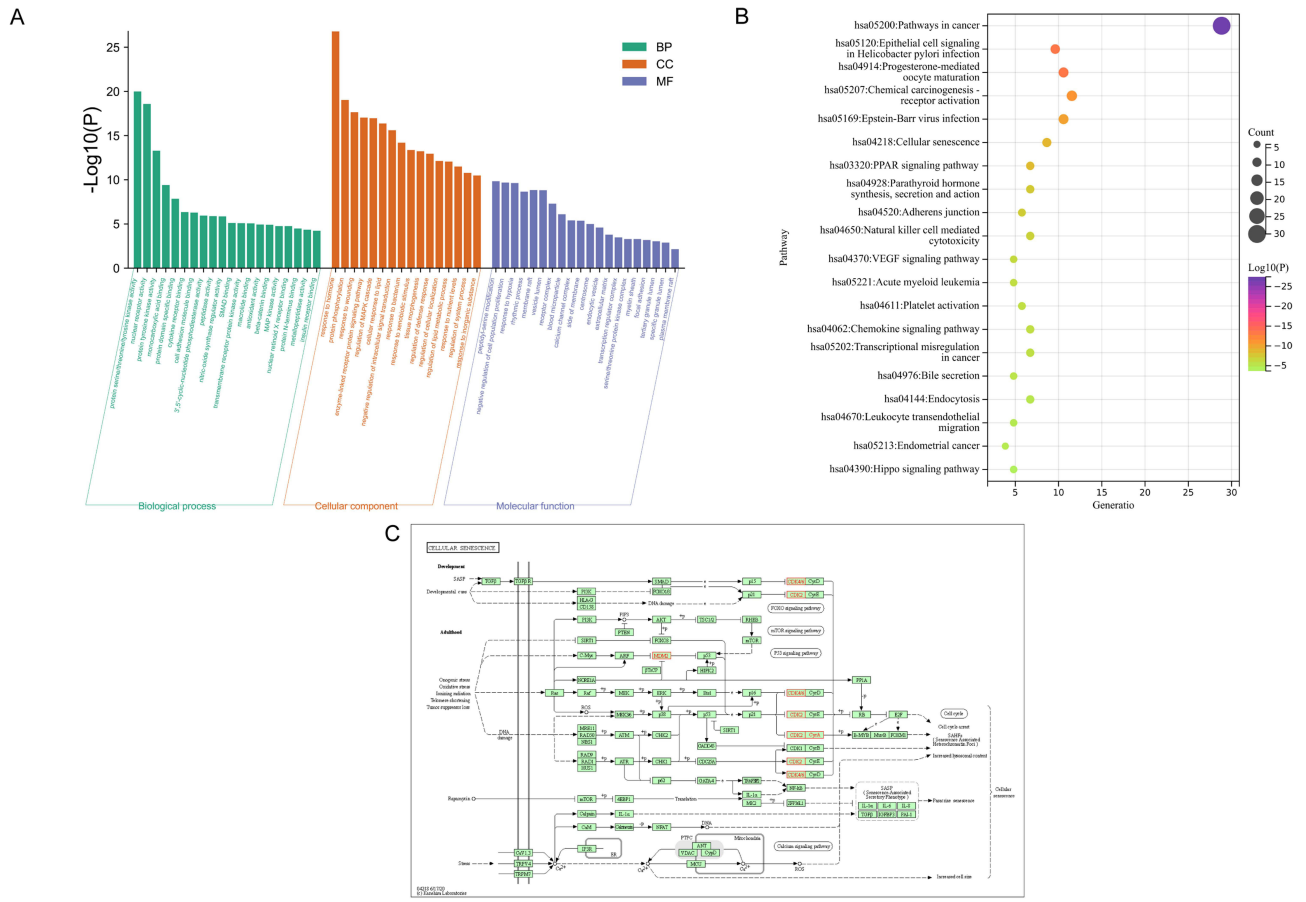

Figure 4 Pathway enrichment analyses. (**A**) GO enrichment analysis. (**B**) KEGG pathway enrichment analysis revealed a strong correlation of cellular senescence pathway. (**C**) KEGG pathway analysis based on hub genes, four hub genes are included in the cellular senescence pathway and directly associated with cellular senescence marker proteins, which are marked with red circles in the figure.

AS-IV Slows PF Development by Attenuating TGF-β1 Production and Thereby Inhibits EMT

Previous studies showed that cellular senescence during PF promotes EMT, which further aggravates PF progression.[26] TGF-β1 is one of the central mediators of fibrosis progression and it can promote EMT. In a bleomycin-induced mouse PF model, our results showed that AS-IV treatment reduced TGF-β1 production, raised E-cadherin protein expression as well as declining Vimentin protein levels compared with the BLM group ($P < 0.05$) (Figure 7). Conclusively, we hypothesized that AS-IV may limit EMT by reducing TGF-β1 production and hence slowing PF progression.

AS-IV Inhibits Bleomycin-Induced Senescence and ROS Production in Alveolar Epithelial A549 Cells

We used bleomycin to establish an A549 cell senescence model based on previous studies. Briefly, 5 μg/mL of bleomycin was used to activate A549 cells for 72 hours.[27] Based on the CCK-8 Cytotoxicity test results, IC_{50}= 128.2uM, we selected different concentrations (12.5,25,50uM) less than the IC_{50} for subsequent cell experiments (Figure 8A). We found that bleomycin treatment significantly changed the morphology of A549 cells, which became flattened. In contrast, when compared to the BLM group, the 50 μM AS-IV treatment significantly reduced the morphological alterations of A549 cells (Figure 8B). Further, the SA-β-Gal assay found that AS-IV significantly delayed the bleomycin-induced senescence in A549 cells (Figure 8C). Excessive production of ROS accelerates cellular senescence, we further explored the cellular senescence-related mechanisms and found that ROS was significantly high in the BLM group, whereas was considerably low in the AS-IV treatment group (Figure 8D). Additionally, we found that AS-IV inhibited the intracellular

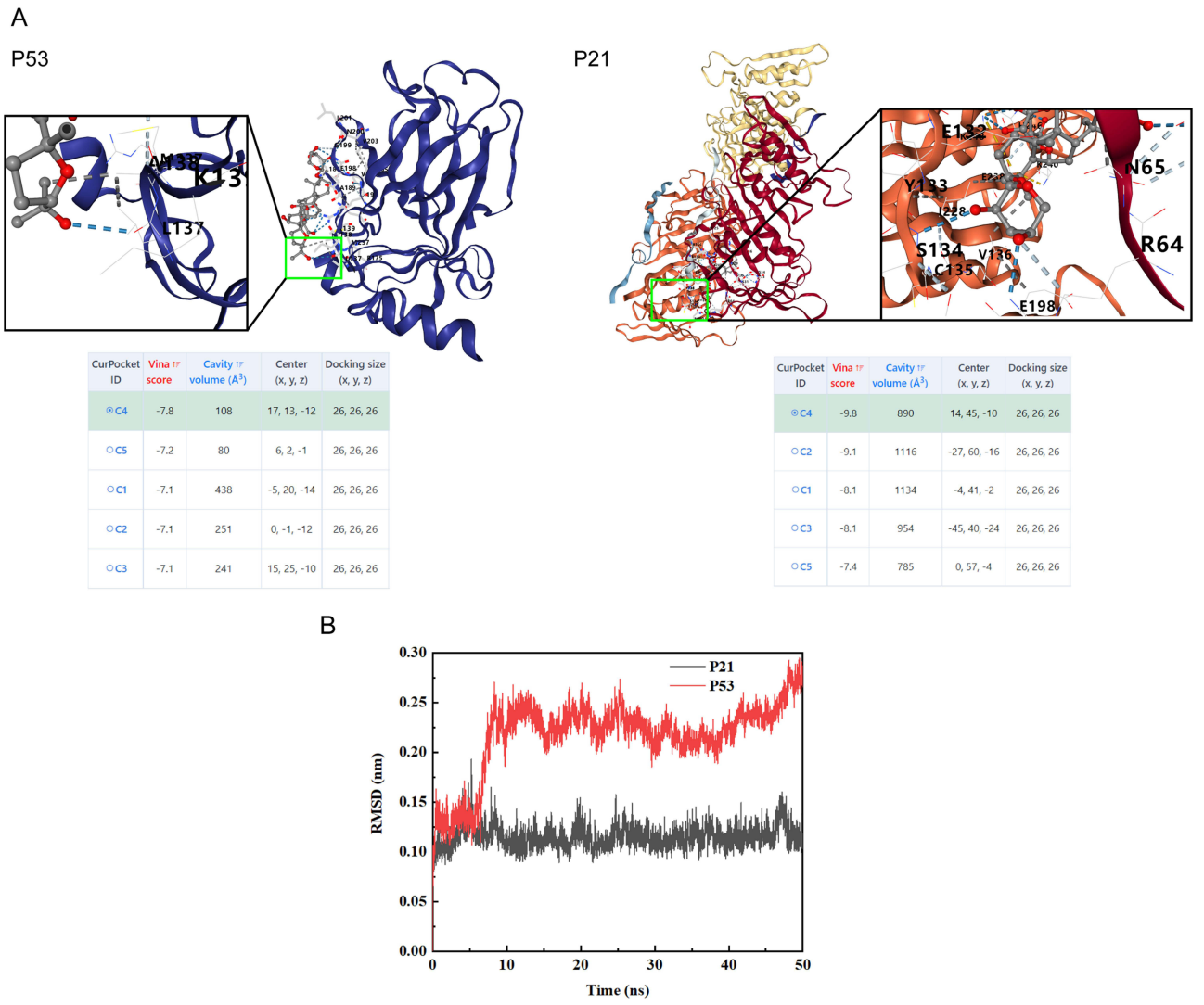

CurPocket ID	Vina score	Cavity volume (Å³)	Center (x, y, z)	Docking size (x, y, z)
C4	-7.8	108	17, 13, -12	26, 26, 26
C5	-7.2	80	6, 2, -1	26, 26, 26
C1	-7.1	438	-5, 20, -14	26, 26, 26
C2	-7.1	251	0, -1, -12	26, 26, 26
C3	-7.1	241	15, 25, -10	26, 26, 26

CurPocket ID	Vina score	Cavity volume (Å³)	Center (x, y, z)	Docking size (x, y, z)
C4	-9.8	890	14, 45, -10	26, 26, 26
C2	-9.1	1116	-27, 60, -16	26, 26, 26
C1	-8.1	1134	-4, 41, -2	26, 26, 26
C3	-8.1	954	-45, 40, -24	26, 26, 26
C5	-7.4	785	0, 57, -4	26, 26, 26

Figure 5 Molecular docking and molecular dynamics simulation. (**A**) Molecular docking revealed that AS-IV has a good binding ability with p53 and p21. The blue dashed line indicates the hydrogen bond. (**B**) Molecular dynamics simulation indicates stable binding of protein ligands.

expression of p53, p21, and p16 proteins in a dose-dependent manner from 0 to 50 μM ($P < 0.001$, $P < 0.001$, $P < 0.01$) (Figure 8E). Conclusively, AS-IV inhibits bleomycin-induced senescence and reduces intracellular ROS production in alveolar epithelial A549 cells.

AS-IV Inhibits EMT in Alveolar Epithelial Cells

We used TGF-β1 to establish an EMT model for A549 cells based on previous studies. Briefly, TGF-β1 at 10 ng/mL was used to stimulate A549 cells for 72 hours.[28] We found that TGF-β1 treatment changed the morphology of A549 cells, which became large and long (Figure 9A). In contrast, 50 μM of AS-IV significantly improved the morphological changes of the cells.

Furthermore, to verify whether AS-IV could retard lung fibrosis by inhibiting EMT, we used the Western blot technique to analyze the expression of epithelial and mesenchymal marker proteins. Different from the TGF-β1 group, the AS-IV group increased the synthesis of E-cadherin, an epithelial protein marker, while decreasing the production of Vimentin, a mesenchymal protein marker, in a dose-dependent manner from 0 to 50 μM ($P < 0.01$, $P < 0.01$) (Figure 9B). In conclusion, AS-IV inhibits EMT in alveolar epithelial A549 cells.

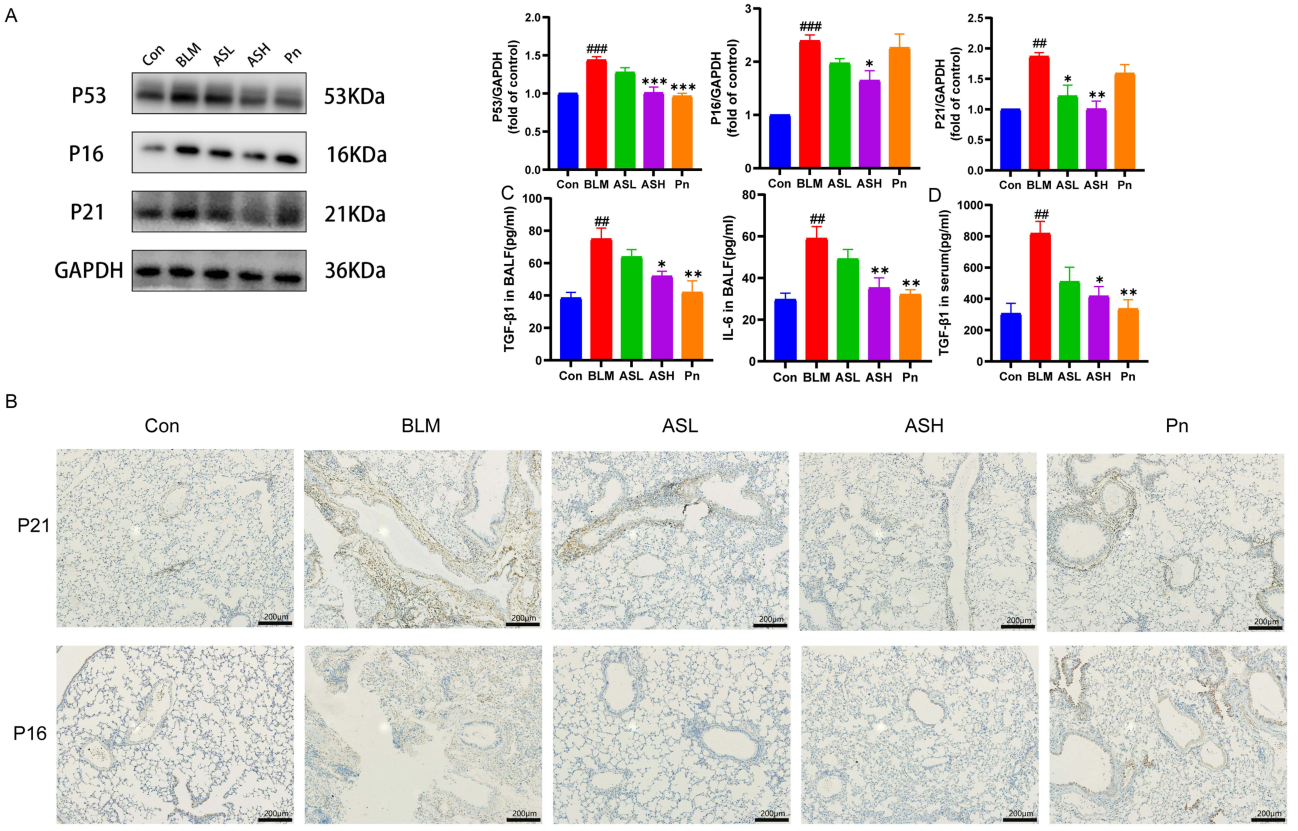

Figure 6 AS-IV attenuates bleomycin-induced alveolar epithelial cell senescence and inflammatory response. (**A**) Western blot of p53, p21, and p16 in lung tissues of fibrotic mice. (**B**) Immunohistochemical staining showed high expressions of p21 and p16 in the BLM group, while reduced expressions of p21 and p16 in the AS-IV group. Scale bar:200um. (**C**) Levels of TGF-β1 and IL-6 in BALF of mice. (**D**) TGF-β1 levels in mouse serum. Data are shown as mean ± SEM (n≥3). ## P < 0.01, #### P < 0.001, vs Con group; * P < 0.05, ** P < 0.01, *** P < 0.001, vs BLM group.

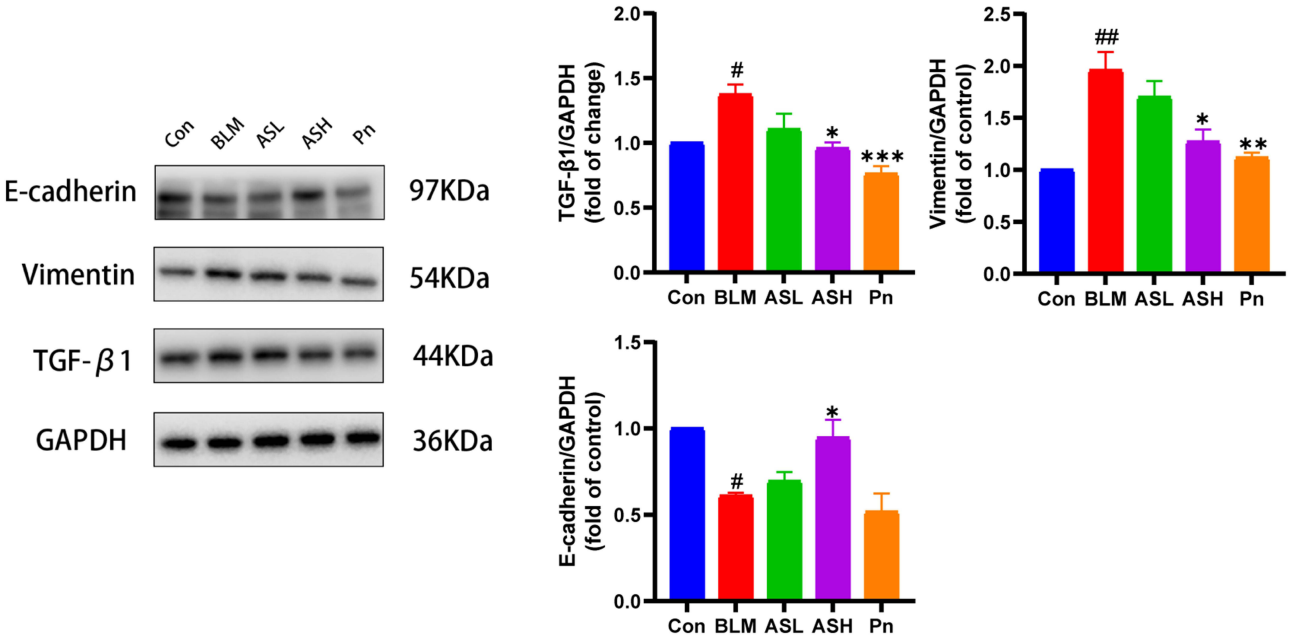

Figure 7 AS-IV attenuates TGF-β1 production and thus inhibits EMT to delay pulmonary fibrosis. Western blot results showed that TGF-β1 was increased in the BLM group, whereas AS-IV treatment reduced its expression. AS-IV group showed upregulated E-cadherin expression and decreased Vimentin expression as compared to the BLM group. Data are shown as mean ± SEM (n≥3). # P < 0.05, ## P < 0.01, vs Con group; * P < 0.05, ** P < 0.01, *** P < 0.001, vs BLM group.

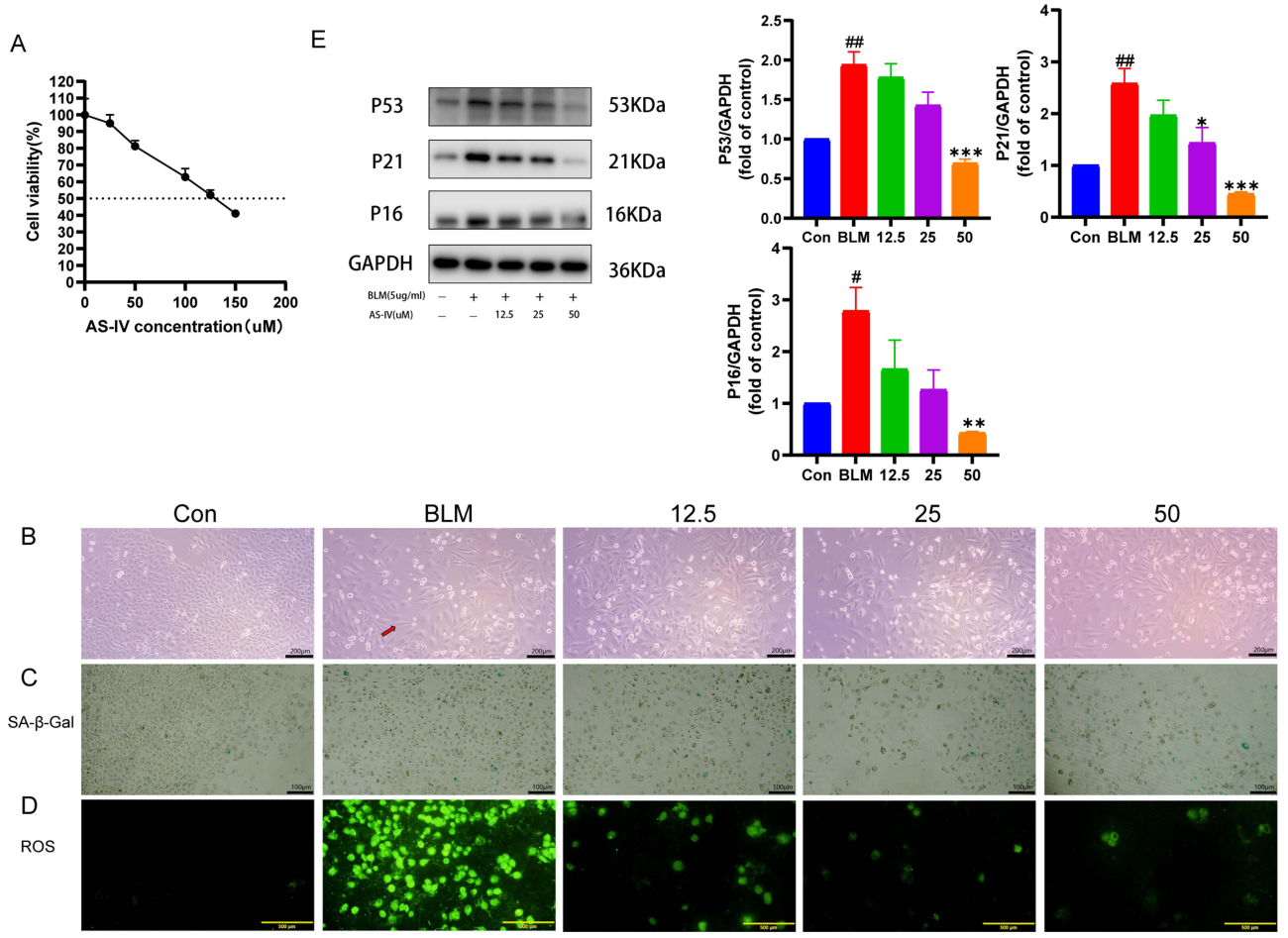

Figure 8 AS-IV inhibits bleomycin-induced senescence and ROS production in alveolar epithelial A549 cells. (**A**) Cytotoxicity of ASIV to A549 cells. (**B**) Morphological plots of each group of A549 cells for 3 days. Red arrows indicate flattened cells. Scale bar:200um. (**C**) SA-β-Gal staining. Scale bar:100um. (**D**) ROS staining indicated that ROS production was significantly high in the BLM group while reduced in the AS-IV group. Scale bar:500um. (**E**) Western blot of p53, p21, and p16 in each group of cells in the BLM-induced senescent A549 cells. Data are shown as mean ± SEM (n≥3). # P < 0.05, ## P < 0.01, vs Con group; * P < 0.05, ** P < 0.01, *** P < 0.001, vs BLM group.

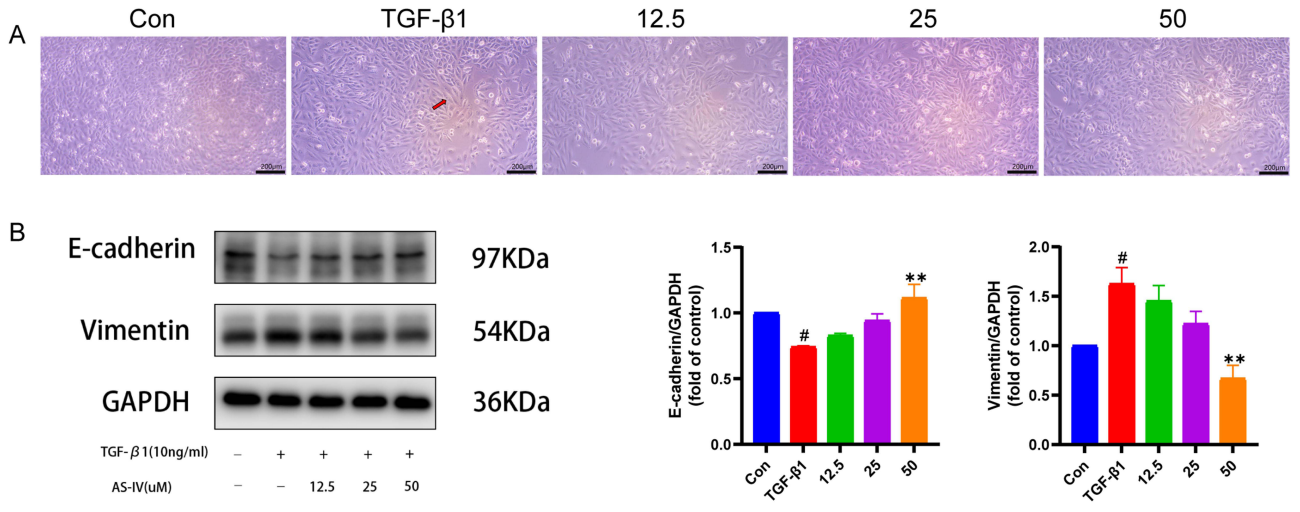

Figure 9 AS-IV inhibits EMT in A549 cells. (**A**) Morphology of A549 cells for 3 days in each group. Red arrow indicates that the cell becomes larger. Scale bar:200um. (**B**) Western blot of E-cadherin and Vimentin in A549 cells EMT model. Data are shown as mean ± SEM (n≥3). # P < 0.05, vs Con group; ** P < 0.01, vs TGF-β1 group.

Discussion

Globally, the treatment of PF has long been a challenge. However, clinically, there is a lack of targeted treatments other than lung transplantation.[29] Although Pirfenidone and Nintedanib are approved by FDA to treat IPF, they do not significantly lower mortality.[30,31] Therefore, it is essential to develop novel PF therapeutic approaches. Accumulating evidence indicates that AS-IV can effectively prevent and treat lung disorders due to its anti-inflammatory, antioxidant, and anti-apoptotic effects.[32] Our study found that AS-IV significantly improved pulmonary fibrosis, and its mechanism of action may be through the inhibition of cellular senescence and EMT.

Collagen is the most important component of the extracellular matrix and is primarily produced by myofibroblasts. Previous research indicated that reducing collagen deposition is an important antifibrosis pathway, while α-SMA is a crucial regulator of fibroblast to myofibroblast transdifferentiation.[33] Strikingly, this study revealed that AS-IV dramatically decreased collagen 1 and α-SMA levels in PF tissues, decreased HYP content in mouse pulmonary tissues, and decreased the aggregation of extracellular matrix in vivo. These findings imply that AS-IV can prevent the deposition of collagen and hence slow PF progression.

Senescence is closely associated with the development and occurrence of PF, and PF incidence increases with age.[34] Cellular senescence includes replicative senescence, caused by DNA damage and activates p53, and stress senescence, caused by oxidative stress damage and activates p16. Interestingly, both these routes activate p21, which inhibits the cell cycle and is a downstream protein-dependent kinase.[35,36] IPF significantly damages the alveolar epithelium, and the aging of this cell population exacerbates PF progression. Using bioinformatics techniques including network pharmacology and molecular docking, AS-IV was predicted to cure PF by preventing cellular senescence. Experimental validation revealed that AS-IV significantly lowered p53, p21, and p16 expressions in lung tissues and considerably ameliorated cellular senescence in the pulmonary tissues of bleomycin-induced PF mice. Furthermore, we used A549 cells as an in vitro alveolar epithelial cell senescence model and observed that bleomycin increased aging in A549 cells with strong positive β-galactosidase staining. Whereas AS-IV treatment significantly reduced cellular senescence. Aging cells are metabolically active and potentially persistent, exhibiting extensive alterations in protein expression and release and ultimately generating SASPs. The term "senescence-messaging secretome" has also been used to describe this trait.[37] Accumulation of senescent cells causes immune system impairment, chronic low-grade lung inflammation, and cellular malfunction through SASPs response. SASPs, in turn, induce cellular senescence, causing senescent cells to release ROS, which further drives senescence progression and aggravates IPF development.[36] Our research found that AS-IV suppressed IL-6 and TGF-β1 levels and attenuated SASPs response. Moreover, we found that AS-IV considerably reduced intracellular ROS production and attenuated mitochondrial damage. These results implicate that AS-IV might be a potent antiaging medication.

Previous research showed that ROS production and SASPs facilitate EMT.[38,39] PF is significantly influenced by EMT, which is activated by TGF-β1.[7,40] EMT is the transformation of epithelial cells to fibroblasts or myofibroblasts. During EMT, numerous epithelial cell biomarkers, including E-calcineurin and occludin, are decreased, while mesenchymal cell biomarkers, including waveform proteins and fibronectin, are increased.[41] In this research, we demonstrated that AS-IV significantly inhibited BLM-induced TGF-β1 expression and mesenchymal protein markers, such as α-SMA and vimentin, while elevated E-cadherin expression in mouse lung tissues. In vitro experiments showed that AS-IV elevated E-cadherin expression while suppressed vimentin expression. These findings are sufficient to demonstrate that AS-IV has significant inhibitory effects on EMT and a slowing effect on PF development.

In summary, our experimental results show that AS-IV has a significant inhibitory effect on pulmonary fibrosis. By combining network pharmacology and molecular docking, we discovered that AS-IV may inhibit the development of pulmonary fibrosis by delaying cell senescence, which we validated in vitro and in vivo. The EMT phenotype is closely related to cell senescence. We found that AS-IV can also inhibit EMT to inhibit pulmonary fibrosis through in vivo and in vitro experiments, proving that AS-IV may delay the development of pulmonary fibrosis by inhibiting cell senescence and EMT. However, our study also has certain limitations. The specific molecular mechanism of AS-IV to improve PF is unknown and needs further investigation.

Conclusion

In summary, our research found that AS-IV could alleviate bleomycin-induced PF by preventing cellular senescence and EMT. This study revealed the potential medicinal value of AS-IV in the treatment of pulmonary fibrosis, providing a basis for the clinical application of AS-IV.

Abbreviations

IPF, Idiopathic pulmonary fibrosis; AS-IV, Astragaloside IV; BLM, bleomycin; EMT, epithelial-mesenchymal transition; CMC, Carboxymethylcellulose; GO, Gene Ontology; KEGG, Kyoto Encyclopedia of Genes and Genomes; PPI, protein–protein interaction; BALF, Broncho Alveolar Lavage Fluid; H&E, Hematoxylin-Eosin stain; HYP, hydroxyproline; IL-6, interleukin 6; TGF-β1, transforming growth factor-β1; PBS, phosphate buffered saline; SDS-PAGE, SDS-polyacrylamide gel electrophoresis; PVDF, polyvinylidene difluoride; ROS, reactive oxygen species; α-SMA, α-smooth muscle actin; SASPs, senescence-associated secretory phenotypes.

Ethics Statement

This study involves human data from public databases called GeneCards. Due to the fact that GeneCards belong to public databases and users can download relevant data for free for research and publish relevant articles, the Ethics Committee of the First Affiliated Hospital of Chongqing Medical University confirms that this study would have had the need for ethics approval waived.

Acknowledgments

This work was supported by the National Natural Science Foundation of China (No. 81573860, No. 82004168), Natural Science Foundation Project of Chongqing (Grant No. cstc2019jcyj-msxmX0180), Kewei Joint Research Project of Chongqing (Grant No. 2019ZY3503). We thank the authors for the development of the database and software used in this paper, we also thank Figdraw (www.figdraw.com) for the assistance in creating flow chart.

Disclosure

The authors report no conflicts of interest in this work.

References

1. Kim HJ, Perlman D, Tomic R. Natural history of idiopathic pulmonary fibrosis. *Respir Med*. 2015;109(6):661–670. doi:10.1016/j.rmed.2015.02.002
2. Richeldi L, Collard HR, Jones MG. Idiopathic pulmonary fibrosis. *Lancet Lond Engl*. 2017;389(10082):1941–1952. doi:10.1016/S0140-6736(17)
3. Qiaolongbatu X, Zhao W, Huang X, et al. The therapeutic mechanism of Schisandrol A and its metabolites on pulmonary fibrosis based on plasma metabonomics and network analysis. *Drug Des Devel Ther*. 2023;17:477–496. doi:10.2147/DDDT.S391503
4. Maher TM, Wells AU, Laurent GJ. Idiopathic pulmonary fibrosis: multiple causes and multiple mechanisms? *Eur Respir J*. 2007;30(5):835–839. doi:10.1183/09031936.00069307
5. Ruaro B, Matucci Cerinic M, Salton F, Baratella E, Confalonieri M, Hughes M. Editorial: pulmonary fibrosis: one manifestation, various diseases. *Front Pharmacol*. 2022;13:765.
6. Confalonieri P, Volpe MC, Jacob J, et al. Regeneration or repair? The role of alveolar epithelial cells in the pathogenesis of idiopathic pulmonary fibrosis (IPF). *Cells*. 2022;11(13):2095. doi:10.3390/cells11132095
7. Phan THG, Paliogiannis P, Nasrallah GK, et al. Emerging cellular and molecular determinants of idiopathic pulmonary fibrosis. *Cell Mol Life Sci*. 2021;78(5):2031–2057. doi:10.1007/s00018-020-03693-7
8. Vancheri C, du Bois RM. A progression-free end-point for idiopathic pulmonary fibrosis trials: lessons from cancer. *Eur Respir J*. 2013;41(2):262–269. doi:10.1183/09031936.00115112
9. Wuyts WA, Wijsenbeek M, Bondue B, et al. Idiopathic pulmonary fibrosis: best practice in monitoring and managing a relentless fibrotic disease. *Respir Int Rev Thorac Dis*. 2020;99(1):73–82. doi:10.1159/000504763
10. Hutchinson J, Fogarty A, Hubbard R, McKeever T. Global incidence and mortality of idiopathic pulmonary fibrosis: a systematic review. *Eur Respir J*. 2015;46(3):795–806. doi:10.1183/09031936.00185114
11. Li L, Hou X, Xu R, Liu C, Tu M. Research review on the pharmacological effects of astragaloside IV. *Fundam Clin Pharmacol*. 2017;31(1):17–36. doi:10.1111/fcp.12232
12. Wang L, Chi YF, Yuan ZT, et al. Astragaloside IV inhibits renal tubulointerstitial fibrosis by blocking TGF-β/Smad signaling pathway in vivo and in vitro. *Exp Biol Med Maywood NJ*. 2014;239(10):1310–1324. doi:10.1177/1535370214532597
13. Wang Z, Li Q, Xiang M, et al. Astragaloside alleviates hepatic fibrosis function via PAR2 signaling pathway in diabetic rats. *Cell Physiol Biochem Int J Exp Cell Physiol Biochem Pharmacol*. 2017;41(3):1156–1166. doi:10.1159/000464122
14. Lu J, Wang QY, Zhou Y, et al. AstragalosideIV against cardiac fibrosis by inhibiting TRPM7 channel. *Phytomedicine Int J Phytother Phytopharm*. 2017;30:10–17. doi:10.1016/j.phymed.2017.04.002
15. Boezio B, Audouze K, Ducrot P, Taboureau O. Network-based approaches in pharmacology. *Mol Inform*. 2017;36:10. doi:10.1002/minf.201700048

16. Kibble M, Saarinen N, Tang J, Wennerberg K, Mäkelä S, Aittokallio T. Network pharmacology applications to map the unexplored target space and therapeutic potential of natural products. *Nat Prod Rep*. 2015;32(8):1249–1266. doi:10.1039/c5np00005j
17. Kelly R, Kidd R. Editorial: chemSpider--a tool for Natural Products research. *Nat Prod Rep*. 2015;32(8):1163–1164. doi:10.1039/c5np90022k
18. Wang X, Shen Y, Wang S, et al. PharmMapper 2017 update: a web server for potential drug target identification with a comprehensive target pharmacophore database. *Nucleic Acids Res*. 2017;45(W1):W356–W360. doi:10.1093/nar/gkx374
19. Stelzer G, Rosen N, Plaschkes I, et al. The GeneCards Suite: from gene data mining to disease genome sequence analyses. *Curr Protoc Bioinforma*. 2016;54:33. doi:10.1002/cpbi.5
20. Szklarczyk D, Franceschini A, Kuhn M, et al. The STRING database in 2011: functional interaction networks of proteins, globally integrated and scored. *Nucleic Acids Res*. 2011;39:D561–568. doi:10.1093/nar/gkq973
21. Chin CH, Chen SH, Wu HH, Ho CW, Ko MT, Lin CY. cytoHubba: identifying hub objects and sub-networks from complex interactome. *BMC Syst Biol*. 2014;8(Suppl 4):S11. doi:10.1186/1752-0509-8-S4-S11
22. Zhou Y, Zhou B, Pache L, et al. Metascape provides a biologist-oriented resource for the analysis of systems-level datasets. *Nat Commun*. 2019;10(1):1523. doi:10.1038/s41467-019-09234-6
23. Liu Y, Yang X, Gan J, Chen S, Xiao ZX, Cao Y. CB-Dock2: improved protein-ligand blind docking by integrating cavity detection, docking and homologous template fitting. *Nucleic Acids Res*. 2022;gkac394. doi:10.1093/nar/gkac394
24. Wang H, Yang T, Wang T, et al. Phloretin attenuates mucus hypersecretion and airway inflammation induced by cigarette smoke. *Int Immunopharmacol*. 2018;55:112–119. doi:10.1016/j.intimp.2017.12.009
25. Aoshiba K, Tsuji T, Nagai A. Bleomycin induces cellular senescence in alveolar epithelial cells. *Eur Respir J*. 2003;22(3):436–443. doi:10.1183/09031936.03.00011903
26. De Blander H, Morel AP, Senaratne AP, Ouzounova M, Puisieux A. Cellular plasticity: a route to senescence exit and tumorigenesis. *Cancers*. 2021;13(18):4561. doi:10.3390/cancers13184561
27. Qiu T, Tian Y, Gao Y, et al. PTEN loss regulates alveolar epithelial cell senescence in pulmonary fibrosis depending on Akt activation. *Aging*. 2019;11(18):7492–7509. doi:10.18632/aging.102262
28. Wan R, Xu X, Ma L, Chen Y, Tang L, Feng J. Novel alternatively spliced variants of Smad4 expressed in TGF-β-induced EMT regulating proliferation and migration of A549 cells. *OncoTargets Ther*. 2020;13:2203–2213. doi:10.2147/OTT.S247015
29. Kistler KD, Nalysnyk L, Rotella P, Esser D. Lung transplantation in idiopathic pulmonary fibrosis: a systematic review of the literature. *BMC Pulm Med*. 2014;14:139. doi:10.1186/1471-2466-14-139
30. Canestaro WJ, Forrester SH, Raghu G, Ho L, Devine BE. Drug treatment of idiopathic pulmonary fibrosis: systematic review and network meta-analysis. *Chest*. 2016;149(3):756–766. doi:10.1016/j.chest.2015.11.013
31. Galli JA, Pandya A, Vega-Olivo M, Dass C, Zhao H, Criner GJ. Pirfenidone and nintedanib for pulmonary fibrosis in clinical practice: tolerability and adverse drug reactions. *Respirol Carlton Vic*. 2017;22(6):1171–1178. doi:10.1111/resp.13024
32. Zhang J, Wu C, Gao L, Du G, Qin X. Astragaloside IV derived from Astragalus membranaceus: a research review on the pharmacological effects. *Adv Pharmacol*. 2020;87:89–112. doi:10.1016/bs.apha.2019.08.002
33. Yang J, Tao L, Liu B, et al. Wedelolactone attenuates pulmonary fibrosis partly through activating AMPK and regulating Raf-MAPKs signaling pathway. *Front Pharmacol*. 2019;10:65.
34. Mora AL, Rojas M, Pardo A, Selman M. Emerging therapies for idiopathic pulmonary fibrosis, a progressive age-related disease. *Nat Rev Drug Discov*. 2017;16(11):755–772. doi:10.1038/nrd.2017.170
35. Hernandez-Segura A, Nehme J, Demaria M. Hallmarks of cellular senescence. *Trends Cell Biol*. 2018;28(6):436–453. doi:10.1016/j.tcb.2018.02.001
36. Barnes PJ, Baker J, Donnelly LE. Cellular senescence as a mechanism and target in chronic lung diseases. *Am J Respir Crit Care Med*. 2019;200(5):556–564. doi:10.1164/rccm.201810-1975TR
37. Coppé JP, Desprez PY, Krtolica A, Campisi J. The senescence-associated secretory phenotype: the dark side of tumor suppression. *Annu Rev Pathol*. 2010;5:99–118. doi:10.1146/annurev-pathol-121808-102144
38. Giannoni E, Parri M, Chiarugi P. EMT and oxidative stress: a bidirectional interplay affecting tumor malignancy. *Antioxid Redox Signal*. 2012;16(11):1248–1263. doi:10.1089/ars.2011.4280
39. Parrinello S, Coppe JP, Krtolica A, Campisi J. Stromal-epithelial interactions in aging and cancer: senescent fibroblasts alter epithelial cell differentiation. *J Cell Sci*. 2005;118(Pt 3):485–496. doi:10.1242/jcs.01635
40. Lamouille S, Xu J, Derynck R. Molecular mechanisms of epithelial-mesenchymal transition. *Nat Rev Mol Cell Biol*. 2014;15(3):178–196. doi:10.1038/nrm3758
41. Singh M, Yelle N, Venugopal C, Singh SK. EMT: mechanisms and therapeutic implications. *Pharmacol Ther*. 2018;182:80–94. doi:10.1016/j.pharmthera.2017.08.009